

# Transition in the geometry of Arctic melt ponds

Christel Hohenegger\*, Bacim Alali\*, Kyle R. Steffen\*,  
Donald K. Perovich<sup>†‡</sup> and Kenneth M. Golden\*

December 23, 2011

## Abstract

During the Arctic melt season, the surface of the sea ice cover undergoes a remarkable transformation from vast expanses of snow covered ice to complex mosaics of ice and melt ponds. Sea ice albedo, a key parameter in climate modeling, is determined by these configurations. However, the seasonal evolution of melt ponds is not well understood, in particular the transition from small ponds to large connected structures. We find here that melt pond evolution exhibits a critical transition from simple Euclidean shapes to self-similar regions whose boundaries resemble fractal space filling curves. By analyzing area–perimeter data from melt pond images, we find that the critical length scale in terms of area is around a hundred square meters. Above this threshold, the fractal dimension of the ponds is close to two as they form larger, more ramified structures and start filling the ice surface. Our findings demonstrate that there are universal features of Arctic melt pond evolution which are similar to phase transitions in statistical physics. They also provide a novel path to simplifying the treatment of melting sea ice in climate models.

## 1 Introduction

Melt ponds on the surface of sea ice form a key component of the late spring and summer Arctic marine environment. While white snow and ice reflect most incident sunlight, melt ponds absorb most of it. The overall albedo of the sea ice pack represents one of the most important parameters in global

---

\*Department of Mathematics, University of Utah, 155 S 1400 E, Salt Lake City, UT 84112-0090 USA

<sup>†</sup>ERDC-CRREL, 72 Lyme Road, Hanover, NH 03755 USA

<sup>‡</sup>Thayer School of Engineering, Dartmouth College, Hanover, NH 03755 USA

climate models. As melting increases so does solar absorption, leading to more melting, and so on, which is called the *ice-albedo feedback*. It is believed that this key feedback effect has played an important role in the precipitous decline observed in summer Arctic sea ice (*Perovich et al.*, 2008).

Despite their importance in climate modeling, comprehensive observations or theories of the formation, coverage, and evolution of melt ponds remain relatively scarce. Available observations of melt ponds show that their areal coverage is highly variable, particularly for first year ice early in the melt season, with rates of change as high as 35% per day (*Scharien and Yackel*, 2005; *Polashenski et al.*, 2011). Such variability, as well as the influence of many competing factors controlling melt pond evolution, makes the incorporation of realistic treatments of albedo into sea ice and climate models quite challenging. There have been substantial efforts at developing detailed small and medium scale models of melt pond coverage which include some of these mechanisms (*Flocco and Feltham*, 2007; *Skyllingstad et al.*, 2009; *Scott and Feltham*, 2010), and at incorporating melt pond parameterizations into global climate models (*Flocco et al.*, 2010; *Hunke and Lipscomb*, 2010; *Pedersen et al.*, 2009).

As an alternative, we ask if the evolution of melt pond geometry exhibits universal characteristics which do not depend on the details of the driving mechanisms. Fundamentally, the melting of Arctic sea ice during summer is a phase transition phenomenon, where solid ice turns to liquid, albeit on large regional scales and over a period of time which depends on environmental forcing and other factors. Thus, we look for features of this important process which are mathematically analogous to related phenomena in the theory of phase transitions. For example, the percolation model for connectedness of the phases in binary composites (*Stauffer and Aharony*, 1992; *Christensen and Moloney*, 2005) exhibits a similar transition in the global geometrical characteristics of the configurations as some parameter is varied.

## 2 Method

The sea ice surface is viewed here as a two phase composite (*Milton*, 2002; *Torquato*, 2002) of dark melt ponds and white snow or ice (Figure 1). We investigate the geometry of the multiscale boundary between the two phases and how it evolves, as well as the connectedness of the melt pond phase. We use two large sets of images of melting sea ice collected during two Arctic expeditions: Healy-Oden TRans Arctic EXpedition (HOTRAX,



Figure 1: Complex geometry of well developed Arctic melt ponds. Aerial photo taken August 14, 2005 on the Healy-Oden Trans Arctic Expedition (HOTRAX). The scale bar represents 75 meters.

2005) (*Perovich et al.*, 2009) and Surface Heat Budget of the Arctic Ocean (SHEBA,1998) (*Perovich et al.*, 2002). The sea ice around SHEBA in the summer of 1998 was predominantly multiyear, with coverage greater than 90% (*Perovich et al.*, 2002). There were a few scattered areas of first year ice, where leads had opened and froze during the winter of 1997-1998. The HOTRAX images from August 14 were of a transition zone between first year and multiyear ice. Ship-based ice observations made on 14 August indicated a 5 to 3 ratio of multiyear to first year ice (*Perovich et al.*, 2009).

After segmenting the images into a three phase system of ice, ocean, and melt ponds (see Appendix A), the melt pond areas and perimeters are computed using the discretized image pixel data and the MATLAB Image Processing Toolbox. Computed in this manner, the area of a melt pond is the total number of pixels corresponding to the melt pond, while the perimeter of a melt pond is the sum of the distances between adjoining pairs of pixels around the border of the melt pond.

### 3 Melt pond connectedness

At the onset of melt pond formation, shallow ponds appear on the ice surface. These initial ponds are rather small on multiyear sea ice but can be more extensive on first year ice. They are generally somewhat circular in shape and their boundaries are simple curves (Figure 2a, photo taken July 8). As melting increases, the area fraction  $\phi$  of the ponds can increase, and the scale over which the melt phase is connected increases rapidly, signaling a percolation threshold at some critical area fraction  $\phi_c$  (*Stauffer and*

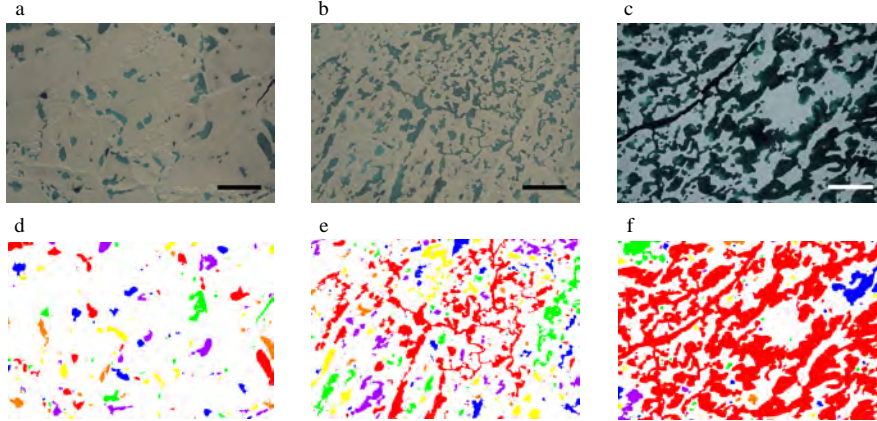


Figure 2: Evolution of melt pond connectivity and color coded connected components. The top row shows melt evolution: (a) disconnected ponds, (b) transition ponds, (c) fully connected melt ponds. The bottom row shows the color coded connected components for the corresponding image above: (d) no single color spans the image, (e) the red phase just spans the image, (f) the connected red phase dominates the image. The scale bars represent 200 meters for (a) and (b), and 35 meters for (c).

*Aharony*, 1992). The value of  $\phi_c$  likely depends on the topography of the ice and snow surface, the age of the ice, and other local characteristics. Similarly, the value of a percolation threshold in a lattice or continuum system depends on the details of the system, such as whether a lattice is square or hexagonal.

While the sets of images we have used allow us to view hundreds of thousands of melt ponds, the dates of the images are restricted to the helicopter flights that were taken on each expedition. Time series of images that are relevant to analyzing the temporal evolution of individual pond structures and their coalescence are not available within these image sets. Nevertheless, the large distances covered by the ship and helicopter, over a significant period of time during the melt season, give us access to quite a large set of possible melt pond configurations and conditions. This set is likely representative of the full ensemble set of possible melt pond configurations exhibited by the sea ice pack, and covers a wide range of melt pond area fractions  $\phi$ .

The transition to ponds which are just barely connected over the scale of the images is illustrated in Figure 2b (photo taken July 8), which has  $\phi \approx 25\%$ . It is reasonable to expect that such a configuration is not so far

from a percolation threshold, and in this particular melting scenario 25% may be a reasonable lower bound on  $\phi_c$ . Exact determination of  $\phi_c$  and its dependence on surface and other conditions requires analysis of melt pond images over length scales larger than are available in our data sets. Above this  $\phi_c$  threshold, the ponds are connected on macroscopic scales much larger than the smaller, individual ponds which form the building blocks of larger structures (Figure 2c, photo taken August 22). Melt ponds whose boundary curve is now convoluted become connected on length scales larger than the available images, and start to fill the entire image space. However, smaller disconnected melt ponds remain during the entire season.

## 4 Fractal geometry of melt ponds

One way of geometrically capturing the transition from small, circular ponds to fully connected large ponds is the fractal exponent  $D$  defined as

$$P \sim \sqrt{A}^D, \quad (1)$$

where  $A$  and  $P$  are the area and perimeter, respectively. For regular objects like circles and polygons, the perimeter scales like the square root of the area, and  $D = 1$ . On the other hand, as the boundary becomes more complex and starts filling the two dimensional space,  $P \sim A$  and thus  $D \approx 2$ . We remark that  $D = 2$  is the upper bound for the two dimensional fractal exponent, since it corresponds to curves which fill two dimensional space (*Sagan, 1994*).

Area-perimeter data were computed for a subset of segmented images for August 22nd (Figure 3, HOTRAX) and we observe a transition between circular ponds with  $D = 1$  and ramified ponds with  $D \approx 2$ . This transition from Euclidean to space filling fractal behavior occurs for ponds of area around a hundred square meters, which is consistent with visual observations made in the Arctic. The transitional length appears to be about the same after analysis of hundreds of thousands of melt ponds from both SHEBA and HOTRAX.

## 5 Discussion

The area-perimeter relation (Figure 3) shows that there is an unexpected separation of scales in melt pond structure. Such findings can ultimately lead to more realistic and efficient treatments of melt ponds in climate models. For example, a natural approach arising from this observation would be a

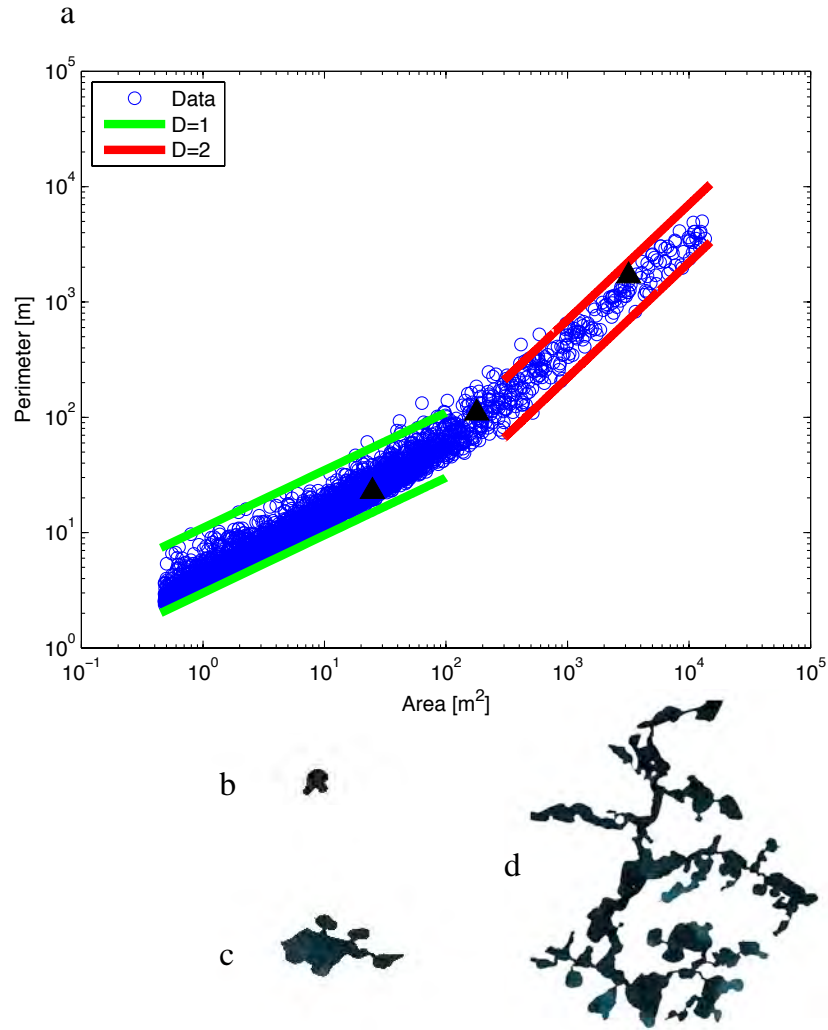


Figure 3: (a) Area-Perimeter data for August 22 (HOTRAX) shows a transition in melt pond fractal dimension from  $D = 1$  to  $D \approx 2$ . The three black triangles, from left to right, correspond to typical ponds in each region: (b) a small pond with  $D = 1$ , (c) a transitional pond with a horizontal length scale of about 29 m, and in (d) a large convoluted pond with  $D \approx 2$ .

multiscale homogenization scheme where the overall albedo of the ice pack is calculated through averaging over appropriate length scales. Interestingly, sea ice floe size distributions display a similar separation of scales with two fractal dimensions (*Toyota et al.*, 2006). Moreover, our findings for the fractal dimension of the melt ponds and its variation are similar to results on the fractal dimensions of connected clusters in percolation and Ising models (*Saleur and Duplantier*, 1987; *Coniglio*, 1989).

Like melt ponds, clouds strongly influence Earth’s albedo. However the geometric structure of clouds and rain areas was found through similar calculations to have a fractal dimension of 1.35 (*Lovejoy*, 1982). This result was constant over the entire range of accessible length scales, which is in stark contrast to what we find here for Arctic melt ponds.

Furthermore, we observe that the critical length scale for melt ponds is determined by the sizes of basic pond shapes which form the building blocks of large scale connected networks. Each melt pond can be broken into basic parts of either thin elongated shapes, which we call bonds, or approximately convex shapes, which we call nodes. Using this terminology, the structure of a melt pond can be described as a locally tree-like network of nodes joined together through bonds. The characteristic feature of a melt pond then becomes its total number of nodes and bonds, rather than its spatial dimensions. A simple melt pond with  $D = 1$  is a small network consisting of a single node or possibly a few connected nodes, while more complex melt ponds are networks consisting of many nodes and bonds. The distinction between transitional ponds ( $1 < D < 2$ ) and complex ponds ( $D \approx 2$ ) is achieved by looking at the self-similarity of melt ponds.

A melt pond is self-similar with respect to its area-perimeter relation if there exists a sub-pond (any connected part of a melt pond that remains after removing some nodes and bonds) such that the perimeter to area ratio of the entire melt pond is approximately the same as that of the sub-pond (Figure 4). For example, by computing the perimeter to area ratios for the original melt pond  $\mathcal{M}$  (Figure 4a) and a sub-pond  $\mathcal{M}_1$  (Figure 4b) we find

$$\frac{P(\mathcal{M})}{A(\mathcal{M})} \approx \frac{P(\mathcal{M}_1)}{A(\mathcal{M}_1)} \approx 0.068 \text{ m}^{-1}. \quad (2)$$

Hence this melt pond is self-similar or complex. On the other hand, transitional ponds are not self-similar. Thus self-similarity allows melt ponds to be classified based on their structure and hence fractal exponent. Moreover, the spatial scales of the transitional ponds determine the transitional scale regime for the fractal dimension.



Figure 4: (a) Melt pond  $\mathcal{M}$ . (b) Sub-pond  $\mathcal{M}_1$ .  $\mathcal{M}$  and  $\mathcal{M}_1$  have the same perimeter to area ratio.  $\mathcal{M}$  is then self-similar or complex with  $D \approx 2$ .

Finally, we remark that in our discussion above on the evolution of melt pond connectivity, we only discussed an initial onset of melting and the subsequent transformation of the surface. However, most observations suggest that ponds actually undergo two of these transitions in time, with massive flooding and full connectivity early in the season. Initial flooding is followed by some drainage and pond shrinkage, with a subsequent increase in pond coverage due to thermal erosion of pond margins and increasing connections. These stages of pond evolution have been discussed in detail by *Eicken et al.* (2002, 2004). The inclusion of such processes in our analysis and the questions they raise will not be considered in this work. Our goal here is to investigate the scaling properties of melt pond geometry that are perhaps insensitive to the specifics of pond history.

Accounting for the complex evolution of Arctic melt ponds and its impact on sea ice albedo is a key challenge to improving projections of climate models. Our results yield fundamental insights into the geometrical structure of melt ponds and how it evolves with increased melting. The separation of scales and fractal structure provides a basis for new approaches to melt pond characterization and the efficient calculation of their role in climate models, as well as a rigorous framework for further investigations.

## A Image segmentation

During the HOTRAX campaign, ten helicopter photographic survey flights following a modified rectangular pattern around the Healy were conducted during the transition from Arctic summer to fall (August-September) at an altitude between 500 and 2000 meters. Images were recorded with a Nikon D70 mounted on the helicopter with the intervalometer set to ten seconds resulting in almost no photo overlaps. During the SHEBA campaign, about a dozen helicopter survey flights following a box centered on the Des Gro-

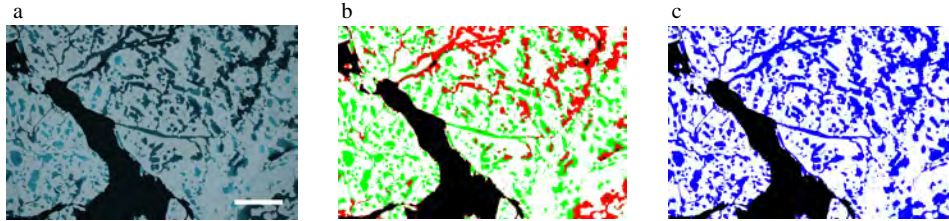


Figure 5: (a) Original image for August 14th (HOTRAX). (b) Four color thresholded image with ice, shallow ponds, deep ponds and ocean/deep ponds colored as white, green, red and black, respectively. (c) Deep and shallow ponds are differentiated from ocean and recombined in the final white, blue and black image for ice, melt ponds and ocean. The scale bar represents 75 meters.

seilliers were conducted between May and October typically at an altitude of 1830 m. Images were recorded with a Nikon 35 mm camera mounted on the back of the helicopter. Again minimal overlap between pictures was seen.

Recorded images show three distinct and geometrically complex features: open ocean, melt ponds and ice. The HOTRAX images are easier to analyze, as the histograms of the RGB pixel values are clearly bimodal. In this case, ice is characterized by high red pixel values, water corresponds to lower red pixel values, while the transition between shallow to deep water follows the blue spectrum from light to dark with ocean being almost black (Figure 5a). The resulting segmentation (Figure 5b) introduces errors as some very deep ponds are mislabeled as ocean. To correct this, the directional derivative of the color intensity in each direction or the change in colors surrounding a deep water region is calculated. If the region is part of a melt pond, the change in color in the original is smooth and the directional derivative is continuous in all directions. A discontinuity reveals the transition from ocean to ice or shallow ponds. In the last step, the correctly labeled shallow and deep ponds are combined to produce a white, blue and black image for ice, melt ponds and ocean (Figure 5c).

**Acknowledgments** :We are grateful for the support provided by the Division of Mathematical Sciences (DMS), the Arctic Natural Sciences (ARC) Program, and the Office of Polar Programs (OPP) at the US National Science Foundation (NSF), through grants DMS-0940249, ARC-0934721, and

DMS-1009704. Kyle Steffen was supported by the Research Experiences for Undergraduates Program through NSF DMS VIGRE grant DMS-0602219 to the Mathematics Department at the University of Utah, as well as a Global Change and Ecosystem Center graduate fellowship at the University of Utah. We also would like to thank Hajo Eicken for valuable comments.

## References

- Christensen, K., and N. R. Moloney (2005), *Complexity and Criticality*, Imperial College Press, London.
- Coniglio, A. (1989), Fractal structure of Ising and Potts clusters: Exact results, *Phys. Rev. Lett.*, *62*(26), 3054–3057, doi:10.1103/PhysRevLett.62.3054.
- Eicken, E., T. C. Grenfell, D. K. Perovich, J. A. Richter-Menge and K. Frey (2004), Hydraulic controls of summer Arctic pack ice albedo, *J. Geophys. Res.*, *109*, C18, C08007.1–C08007.12, doi:10.1029/2006JC003836.
- Eicken, E., H. R. Krouse, D. Kadko, and D. K. Perovich (2002), Tracer studies of pathways and rates of meltwater transport through Arctic summer sea ice, *J. Geophys. Res.*, *107*, C10, 8046, doi:10.1029/2000JC000583.
- Flocco, D., and D. L. Feltham (2007), A continuum model of melt pond evolution on Arctic sea ice, *J. Geophys. Res.*, *112*, C08, 016, doi:10.1029/2006JC003836.
- Flocco, D., D. L. Feltham, and A. K. Turner (2010), Incorporation of a physically-based melt pond scheme into the sea ice component of a climate model, *J. Geophys. Res.*, doi:10.1029/2009JC005568.
- Hunke, E. C., and W. H. Lipscomb (2010), *CICE: the Los Alamos Sea Ice Model. Documentation and Software User’s Manual. Version 4.1*, T-3 Fluid Dynamic Group, Los Alamos National Laboratory, Los Alamos.
- Lovejoy, S. (1982), Area-perimeter relation for rain and cloud areas, *Science*, *216*, 185–187, doi:10.1126/science.216.4542.185.
- Milton, G. W. (2002), *Theory of Composites*, Cambridge University Press, Cambridge.

- Pedersen, C. A., E. Roeckner, M. Lüthje, and J. Winther (2009), A new sea ice albedo scheme including melt ponds for ECHAM5 general circulation model, *J. Geophys. Res.*, *114*, D08,101, doi:10.1029/2008JD010440.
- Perovich, D. K., W. B. Tucker III, and K. A. Ligett (2002), Aerial observations of the evolution of ice surface conditions during summer, *J. Geophys. Res.*, *107*(C10), doi:10.1029/2000JC000449.
- Perovich, D. K., J. A. Richter-Menge, K. F. Jones, and B. Light (2008), Sunlight, water, and ice: Extreme Arctic sea ice melt during the summer of 2007, *Geophys. Res. Lett.*, *35*, L11,501, doi:10.1029/2008GL034007.
- Perovich, D. K., T. C. Grenfell, B. Light, B. C. Elder, J. Harbeck, C. Polashenski, W. B. T. III, and C. Stelmach (2009), Transpolar observations of the morphological properties of Arctic sea ice, *J. Geophys. Res.*, *114*, C00A04, doi:10.1029/2008JC004892.
- Polashenski, C. M., D. K. Perovich, and Z. Courville (2011), The mechanisms of sea ice melt pond formation and evolution, *J. Geophys. Res.*, doi:10.1029/2011JC007231, in press.
- Sagan, H. (1994), *Space-Filling Curves*, Springer Verlag, New York.
- Saleur, H., and B. Duplantier (1987), Exact determination of the percolation hull exponent in two dimensions, *Phys. Rev. Lett.*, *58*(22), 2325–2328, doi:10.1103/PhysRevLett.58.2325.
- Scharien, R. K., and J. J. Yackel (2005), Analysis of surface roughness and morphology of first-year sea ice melt ponds: Implications for microwave scattering, *IEEE Trans. Geosci. Rem. Sens.*, *43*, 2927, doi:10.1109/TGRS.2005.857896.
- Scott, F., and D. L. Feltham (2010), A model of the three dimensional evolution of Arctic melt ponds on first year and multiyear sea ice, *J. Geophys. Res.*, *115*, C12,064, doi:10.1029/2010JC006156.
- Skyllingstad, E. D., C. A. Paulson, and D. K. Perovich (2009), Simulation of melt pond evolution on level ice, *J. Geophys. Res.*, *114*, C12,019, doi:10.1029/2009/2009JC005363.
- Stauffer, D., and A. Aharony (1992), *Introduction to Percolation Theory, Second Edition*, Taylor and Francis Inc., Philadelphia.

Torquato, S. (2002), *Random Heterogeneous Materials: Microstructure and Macroscopic Properties*, Springer-Verlag, New York.

Toyota, T., S. Takatsuji, and M. Nakayama (2006), Characteristics of sea ice floe size distribution in the seasonal ice zone, *Geophys. Res. Lett.*, *33*, L02,616, doi:10.1029/2005GL024556.